Int. J. Heat Mass Transfer. Vol. 18, pp. 635–648. Pergamon Press 1975. Printed in Great Britain

THE EFFECT OF UPPER SURFACE CONDITIONS ON CONVECTION IN A SHALLOW CAVITY WITH DIFFERENTIALLY HEATED END-WALLS

D. E. CORMACK, G. P. STONE and L. G. LEAL
Chemical Engineering, California Institute of Technology, Pasadena, California 91109, U.S.A.

(*Received* 5 *October* 1973 *and in revised form* 13 *August* 1974)

Abstract—The effect of upper surface boundary conditions on the flow structure in shallow cavities with differentially heated end-walls is examined. Matched asymptotic solutions, valid for small cavity aspect ratios are presented for the following cases; uniform shear stress with zero heat flux, uniform heat flux with zero shear stress, and heat flux linearly dependent on surface temperature with zero shear stress. It is shown that these changes in surface boundary conditions have an important influence on the temperature and flow structure within the cavity.

NOMENCLATURE

A, aspect ratio, $= h/l$;
B, dimensionless shear parameter $= l\tau_0/h^2(T_h - T_c)\beta g$;
c_i, c_i', coefficients which are functions of Gr and Pr;
c_p, heat capacity;
$F(y)$, $y^5/120 - 5y^4/192 + y^3/48$;
$f(T)$, surface heat flux;
Gr, Grashof number, $= \beta g(T_h - T_c)h^3/\nu^2$;
H, scaled thermal exchange coefficient, $= Kh/kA^2$;
h, cavity depth;
K, effective thermal exchange coefficient;
K_1, K_2, core solution parameters;
k, thermal conductivity;
l, cavity length;
l', characteristic length for surface heat transfer;
Nu, Nusselt number, $= \int_0^1 \left.\frac{\partial\theta}{\partial x}\right|_{x=0} dy$;
Pr, Prandtl number, $= c_p\mu/k$;
Q, scaled surface heat flux, $= qh/kA^2(T_h - T_c)$;
q, surface heat flux;
T_c, T_h, cold- and hot-end wall temperatures;
T_e, equilibrium temperature for surface heat transfer;
u^*, slip velocity;
x, y, cartesian coordinates nondimensionalized by h;
$\hat{x}$, Ax.

Greek symbols

β, coefficient of thermal expansion;
ε, $\sqrt{(Kh/k)}$;
η, $(1-y)$;
Θ, $(1-\theta)$;
θ, $(T - T_c)/(T_h - T_c)$;
μ, viscosity;
ν, kinematic viscosity;
ξ, horizontal distance from hot end of cavity, $= A^{-1} - x$;
$\bar{\xi}$, core variable for semi-infinite cavity, $= \varepsilon\xi$;
τ_0, surface kinematic shear stress;
Ω, hot end vorticity;
ω, vorticity;
Ψ, hot end stream function;
ψ, stream function.

1. INTRODUCTION

IT HAS become a common practice to use estuaries and other bodies of water for the disposal of the waste heat that arises as a by-product of fossil and atomic fuel electric power generation. Similarly, sewage treatment plants often discharge high concentrations of organic pollutants directly into estuaries and coastal waters. Although such dumping may be safely carried out, it is important to take proper consideration of its impact on the biochemical processes that depend critically on the water temperature and purity. As a first step toward understanding the biological impact, laboratory and field experiments have established practical temperature and toxicity limits, beyond which the biological processes are impaired. However, before outfall systems can be designed so that these limits are not exceeded, it is necessary to understand more fully the mechanisms by which these wastes are dispersed within the body of water.

Estuaries which are shallow (depth much smaller than length) and have strong enough vertical mixing to prevent the formation of density wedges, often exhibit a density distribution which is vertically uniform but which varies approximately linearly in the horizontal direction. An excellent naturally occurring example is Shark Bay on the West Australian coast (Logan and Cebulski [1]). More commonly, perhaps, the horizontal gradient may be established as a result of man-related heat input near the end of the estuary. In either case, the slow gravitational circulation, induced by the horizontal density gradient, can contribute significantly to the longitudinal dispersion of pollutants, mainly by the mechanism of Taylor diffusion (Fischer [2]).

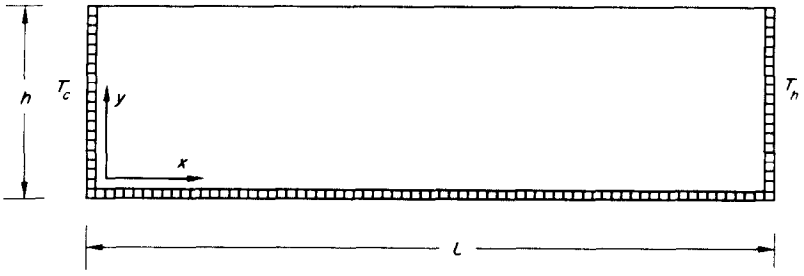

FIG. 1. Schematic diagram of the cavity.

A complete dynamic model of an estuary such as Shark Bay would, of course, be very complex. The geometry of the estuary is complicated, and the flow is turbulent and generally coupled with the tidal cycle. Furthermore, various regions of the flow field are controlled by processes occurring on very different length scales. In the immediate vicinity of the source (for example, near the discharge of heated fluid from a power plant) the problem is dominated by the details of the source geometry, and the *local* mixing processes (cf. Harleman and Stolzenbach [3]). Covering a much wider area beyond this so-called "near-field" region, is the region of interest in the present work, namely the "far-field," where the primary transport mechanisms are bulk diffusion and convection. In this region, the detailed velocity and density fields are relatively insensitive to the source configuration. In addition, since the time scale of the gravitational circulation in the far-field is large, the influence of the tidal cycle and other unsteady variations of velocity on the mean circulation in the estuary may be taken into account by the use of effective eddy exchange coefficients (Imberger [4]). Thus, considerable insight into the basic far-field flow structure can be obtained from the idealized problem of *laminar* flow in a shallow two-dimensional cavity with differentially heated end walls.

Investigations into the problem of natural convection in two-dimensional cavities have been extensive. Most theoretical studies have focused on numerical solutions of the full equations of motion, subject to the Boussinesq approximation, for cavities which are either square or have a depth, h, larger than their length, l (cf. Quon [5], Wilkes and Churchill [6], Newell and Schmidt [7] and DeVahl Davis [8]). Notably, these studies have not dealt specifically with the case of *small* aspect ratio ($A \equiv h/l \ll 1$) which is relevant to the estuary circulation problem. In a recent paper, Cormack, Leal and Imberger [9] provided an analytical description of the convective motion of a Newtonian fluid in a two-dimensional enclosed cavity with a rigid, no-slip, insulating lid for the limiting case $A \to 0$, with fixed values of the Grashof number, Gr. The basic features of shallow cavity flow, as predicted by this theory, were subsequently verified both by numerical solutions of the full equations of motion (Cormack, Leal and Seinfeld [10]), and by experimental measurements (Imberger [4]).

As explained by Imberger [4], the no-slip insulating boundary was the only surface condition for which reliable laboratory data could be obtained, and this motivated its use in our previous analytical investigation. Clearly, this condition is quite different from that relevant to an open surface estuary, and the effect of this difference upon the circulation dynamics is not obvious. It is the purpose of the present study to investigate this question for the more realistic conditions of an imposed surface shear stress (due, for example, to a surface wind stress) and surface heat transfer. The analysis will show that these modifications of the boundary conditions can have a very significant effect on the Nusselt number (and hence on the longitudinal dispersive capacity of the cavity) as well as on the form of the velocity and temperature profiles for $A \to 0$, with other parameters held fixed.*

2. MATHEMATICAL FORMULATION OF THE PROBLEM

The system that we consider is shown schematically in Fig. 1. It consists of a cavity of length, l, and height, h, that contains a Newtonian fluid. The end walls are held at different, but uniform temperatures, T_c and T_h, with $T_c < T_h$. The bottom of the box is insulated and the end walls and bottom are rigid, no-slip boundaries. At the upper surface, the kinematic shear stress is assumed to have some uniform value, τ_0, and the heat flux is given as a function of the surface temperature, $f(T)$.

Subject to the usual Boussinesq approximation, the steady-state equations governing this system may be expressed (see [9]) as

$$GrA^2 \frac{\partial(\omega, \psi)}{\partial(x, y)} = A\nabla^2\omega + \frac{\partial\theta}{\partial x} \tag{1}$$

$$\nabla^2\psi = -\omega \tag{2}$$

$$PrGrA \frac{\partial(\theta, \psi)}{\partial(x, y)} = \nabla^2\theta \tag{3}$$

with boundary conditions

$$\left.\begin{aligned} &\psi = 0, \quad \frac{\partial\psi}{\partial x} = 0, \quad \theta = Ax \quad \text{on} \quad x = 0, A^{-1} \\ &\psi = 0, \quad \frac{\partial\psi}{\partial y} = 0, \quad \frac{\partial\theta}{\partial y} = 0 \quad \text{on} \quad y = 0 \end{aligned}\right\} \tag{4}$$

*In contrast, for $Gr \to \infty$, A fixed, the recent numerical solutions of Quon [5] indicate that the upper surface condition for the velocity plays a less important role, at least in determining Nu.

and

$$\frac{\partial \psi}{\partial x} = 0, \quad \frac{\partial^2 \psi}{\partial y^2} = \frac{l\tau_0}{h^2(T_h - T_c)\beta g},$$

$$\frac{\partial \theta}{\partial y} = \frac{hf(T)}{k(T_h - T_c)} \quad \text{on} \quad y = 1. \quad (5)$$

To nondimensionalize these equations, we have used h as the characteristic length scale, and $\beta g(T_h - T_c)h^3/\nu l$ as the characteristic velocity. Although perhaps not obvious, this velocity scaling is the most convenient choice for the present problem, where the basic flow structure is found to consist of a buoyancy driven parallel flow which is moderated by viscous effects over a length l. At any rate, it may be justified *a posteriori* by the theory which is presented in this paper. The dimensionless parameters which appear in the equations (1)–(3) are the Grashof number Gr, the Prandtl number Pr, and the cavity aspect ratio. The additional dimensionless parameters introduced as a result of the surface conditions (5), will be discussed in the body of the paper.

3. THE NO-SLIP, INSULATED CAVITY

Before the general case represented by (5) is considered, it is useful to summarize the basic analytical techniques and results obtained in [9], for the no-slip insulated cavity. The key simplifying feature in this case is the assumption, supported by experimental observation, that the length scale for horizontal change in the central region of the cavity is $O(A)^{-1}$, while the scale for horizontal change near the end walls is only $O(1)$. Because this disparity in length scales increases as $A \to 0$, an analytic solution to (1)–(5) may be obtained using the standard methods of matched asymptotic expansions, in the limit $A \to 0$ with the other parameters held fixed. Analytically, the cavity is decomposed into three parts, a core region of extent $O(A^{-1})$ in the center of the cavity, and two end regions within an $O(1)$ distance of the end walls. The solutions in the three regions are coupled by the matching requirements in the regions of overlap.

The core solution is easily obtained by introducing the scaling

$$\hat{x} = Ax \quad (6)$$

into the governing equations and boundary conditions (1)–(5), and expanding the streamfunction and temperature as regular series in the small parameter A

$$\left.\begin{aligned} \psi &= \psi_0 + A\psi_1 + A^2\psi_2 + \dots \\ \theta &= \theta_0 + A\theta_1 + A^2\theta_2 + \dots \end{aligned}\right\} \quad (7)$$

The resulting solution is

$$\psi = K_1(y^4/24 - y^3/12 + y^2/24) \quad (8)$$

$$\theta = K_1\hat{x} + K_1^2 GrPrA^2(y^5/120 - y^4/48 + y^3/72) + K_2 \quad (9)$$

where

$$\left.\begin{aligned} K_1 &= c_1 + Ac_2 + A^2c_3 + \dots \\ K_2 &= c_1' + Ac_2' + A^2c_3' + \dots \end{aligned}\right\} \quad (10)$$

The coefficients $c_1, c_2, \dots, c_1', c_2', \dots$ are determined by matching the core solution with solutions valid in the end regions. Because of the symmetry of equations (1)–(4) and the no-slip, insulated boundary conditions, the coefficients c_i' can be eliminated in favor of the single set c_i, so that the matching operation reduces to a consideration of solutions valid in the cold end of the cavity. Upon calculating the end region solutions and carrying out the matching, the coefficient K_1, governing the magnitude of the horizontal temperature gradient in the core, was found to be

$$K_1 = 1 - 3{\cdot}48 \times 10^{-6} Gr^2 Pr^2 A^3 + O(Gr^4 Pr^4 A^5) \quad (11)$$

while the Nusselt number,

$$Nu \equiv \int_0^1 \left.\frac{\partial \theta}{\partial x}\right|_{x=0} \mathrm{d}y$$

was shown to be of the form

$$Nu = A + 2{\cdot}86 \times 10^{-6} Gr^2 Pr^2 A^3 + O(Gr^2 Pr^2 A^4). \quad (12)$$

The corresponding stream function representing the first order flow field in the (cold) end region is shown in Fig. 2(a).

Solutions (8) and (9) indicate that the core flow for a no-slip insulated surface is parallel to all orders of magnitude in A, while, to first order in A, the temperature is linear in $\hat{x}$ and independent of y. Thus, to a first approximation, the end regions are isothermal and the driving force for convection is associated with the horizontal gradient of θ in the core. The end regions serve mainly to turn the core flow through 180° as required by the condition of zero volume flux through the end walls. In these features the flow associated with the limit $A \to 0$ with Gr fixed (though perhaps large) is fundamentally different from that appropriate to the limit A fixed (though perhaps small) and $Gr \to \infty$ which was studied by Gill [11]. In the latter case, nearly all of the temperature drop occurs in thin end wall boundary layers and the corresponding gradients constitute the primary driving force for fluid motion. In particular, the core flow exists *only* as a consequence of the entrainment–detrainment process associated with the end wall boundary layers.

It is also significant that the longitudinal heat-transfer process in the present case is dominated by conduction [cf. equations (9) and (12)], and that this occurs for any arbitrary Grashof number provided only that A is made sufficiently small. Clearly, the problem considered here differs in a fundamental way from the usual conduction limit A fixed, $Gr \to 0$. In the present case, as A is decreased the horizontal scale of the cavity increases relative to its depth so that even the small viscous contributions associated with a large value of Gr can eventually become important and effectively "throttle" the flow, thus enhancing conduction compared with convection in the core region.

Finally, it may be noted that the higher order *convective* contributions to (9) and (12) are a result of the Taylor diffusion mechanism which has been

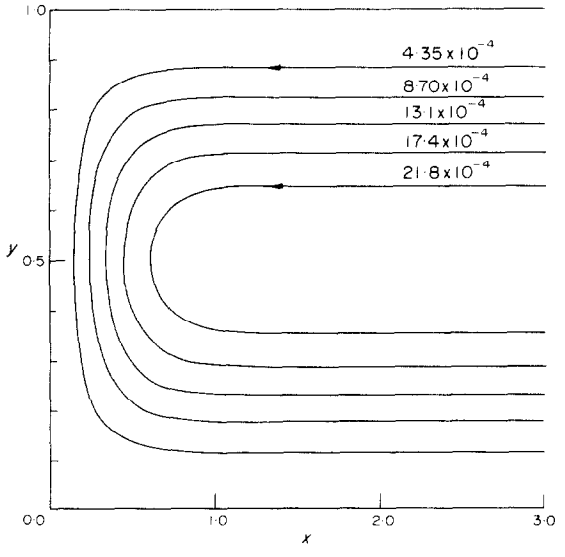

(a) Fixed lid.

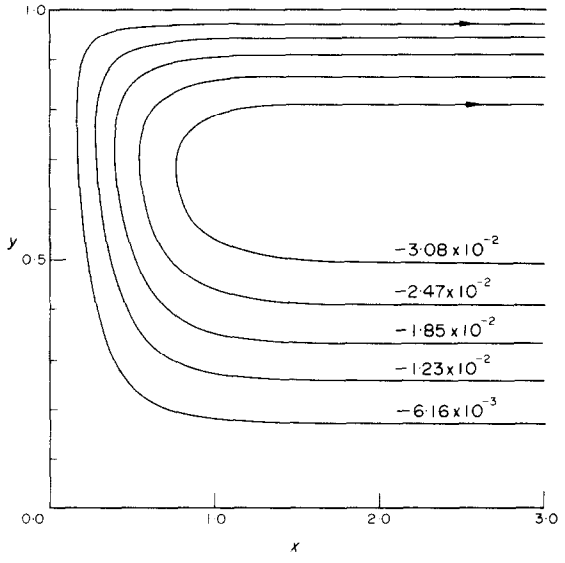

(b) Imposed shear stress.

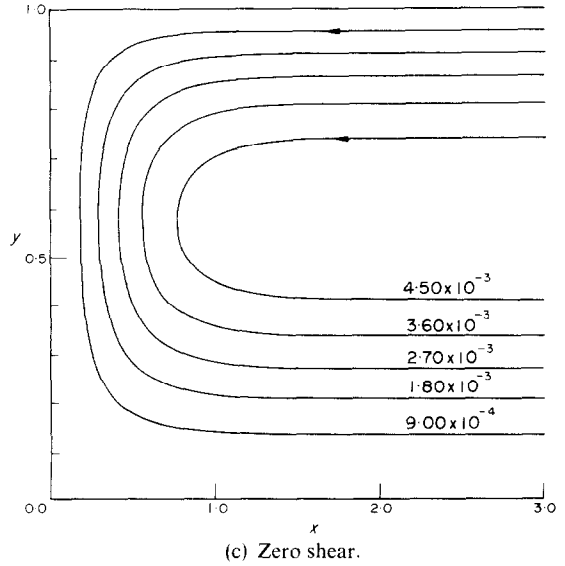

(c) Zero shear.

FIG. 2. Streamlines in cold end.

recently reviewed in the context of cavity and estuary flows, by Fischer [12].†

In the following sections we consider the changes in flow structure which occur as the no-slip, insulated upper surface conditions are replaced by the conditions (5).

4. ASYMPTOTIC VELOCITY AND TEMPERATURE FIELDS WITH AN IMPOSED SURFACE SHEAR STRESS AND ZERO HEAT FLUX

The logical extension of the no-slip upper surface, which was discussed in [9] and summarized in the previous section, is the case of an imposed, uniform shear stress, τ_0. The problem differs from the previous one only in the condition

$$\frac{\partial^2\psi}{\partial y^2} = \frac{l\tau_0}{h^2(T_h - T_c)\beta g} = B \quad \text{on} \quad y = 1 \tag{13}$$

which replaces the no-slip condition, $\partial\psi/\partial y = 0$. In natural estuaries, τ_0 could be interpreted as the time- and space-averaged value of the surface wind shear stress. In that case, a typical range for τ_0 would be $0-10\,\text{cm}^2/\text{s}^2$ (cf. Lumley and Panofsky [13]), which leads to the estimate $0 \lesssim |B| \lesssim 2$ in Shark Bay. The dimensionless parameter B provides a measure of the relative magnitudes of the surface shear force and the characteristic buoyancy force in the cavity. When $B \ll 1$, the buoyancy forces are dominant and the problem is equivalent to the case $\tau_0 = 0$. On the other hand, for $B \gg 1$, the shear forces are dominant and the problem is a forced convection flow to first approximation. It is the intermediate case, $B \sim O(1)$, which we will pursue here. The analysis follows that in [9] fairly closely. Thus, in the interest of brevity, we omit the details of the end region solutions and of the matching. The relevant techniques are demonstrated in the Appendix for the somewhat simpler but representative case of $B = 0$. Here, we shall concentrate on the solutions themselves rather than on the methods used to obtain them.

In the core region,

$$\psi = K_1\left(\frac{y^4}{24} - \frac{5y^3}{48} + \frac{y^2}{16}\right) + \frac{B}{4}(y^3 - y^2) \tag{14}$$

$$\theta = K_1\hat{x} + PrGrA^2\left\{K_1^2\left(\frac{y^5}{120} - \frac{5y^4}{192} + \frac{y^3}{48}\right) + K_1 B\left(\frac{y^4}{16} - \frac{y^3}{12}\right)\right\} + K_2 \tag{15}$$

where K_1 and K_2 are polynomials in A. The coefficients of K_1 and K_2 depend on Gr, Pr, A and B, and are determined by matching (14) and (15) with the solutions in the two end regions. The principal feature of interest in the latter (end region solutions) is the fact that the surface shear stress yields only a simple additive contribution at first order in A.

$$\psi = \psi_0 + B\hat{\psi}_0 + O(A).$$

†The convective terms in these equations can, in fact, be reproduced using the general equations (10) and (12) of Fischer's paper.

The first term, ψ_0, is simply the $\tau_0 = 0$ solution outlined in the Appendix. The second term, $\hat{\psi}_0$, which is directly attributable to the imposed surface shear stress, was obtained numerically. The governing equation and boundary conditions are

$$\nabla^4 \hat{\psi}_0 = 0 \tag{16}$$

$$\left.\begin{aligned} &\hat{\psi}_0 = 0 \quad \text{on} \quad x = 0 \quad \text{on} \quad y = 0, 1 \\ &\frac{\partial \hat{\psi}_0}{\partial y} = 0 \quad \text{on} \quad y = 0; \quad \frac{\partial \hat{\psi}_0}{\partial x} = 0 \quad \text{on} \quad x = 0, \infty \\ &\frac{\partial^2 \hat{\psi}_0}{\partial y^2} = 1 \quad \text{on} \quad y = 1. \end{aligned}\right\} \tag{17}$$

The numerical scheme closely resembled that described in the Appendix for ψ_0. Typical streamlines for $\hat{\psi}_0$ are presented in Fig. 2(b).

To determine K_1 and Nu to $O(A^3)$, in addition to the five end region temperature corrections obtained in the Appendix for $\tau_0 = 0$, three additional corrections had to be calculated; one at $O(A^2)$ and two at $O(A^3)$. The resulting expression for K_1, correct to $O(A^3)$, is

$$K_1 = 1 - Pr^2 Gr^2 A^3 (19{\cdot}16 \times 10^{-6} - 2{\cdot}536 \times 10^{-4} B + 8{\cdot}550 \times 10^{-4} B^2) + O(A^4). \tag{18}$$

Similarly, the Nusselt number (12) is modified to

$$Nu_{\tau_0} = A + Pr^2 Gr^2 A^3 (13{\cdot}10 \times 10^{-6} - 1{\cdot}736 \times 10^{-4} B + 5{\cdot}952 \times 10^{-4} B^2) + O(A^4). \tag{19}$$

Our primary interest in the results of the preceding analysis is with the qualitative variations in flow structure which are induced by changes in boundary conditions at the upper surface. Most relevant to the far-field aspects of estuary flows are the structure of the core flow and the magnitude of the first correction $[O(A^3)]$ to the Nusselt number, since the latter is a measure of the rate of longitudinal convective transport in the cavity. In this regard, the most important conclusion from the solutions (14)–(19) is the absence of any fundamental change in the flow structure for nonzero B. The parallel flow in the core region is preserved for any fixed value of B in the limit as $A \to 0$. In addition, the temperature field, which is dominated at first order by the basic conduction mechanism, remains linear in the horizontal coordinate in all cases with the y-dependence of the temperature field (and therefore the vertical density stratification) entering only as a higher order, $O(A^2)$, term. Finally, the fundamental Taylor diffusion mechanism which dominates the convective heat-transfer process in the core is again reflected in the basic forms of the temperature gradient, K_1, and the Nusselt number. In spite of these basic similarities, however, the detailed temperature and velocity distributions vary substantially with changes in B, and these changes are accompanied by important variations in the capacity for longitudinal convective transport of heat.

The most obvious variations in the core flow are those associated with the velocity profile. In Fig. 3 we compare the normalized velocity profiles for the no-slip boundary condition $(y^3/6 - y^2/4 + y/12)$ and the free shear condition $(y^3/6 - 5y^2/16 + y/8)$. Also plotted is the

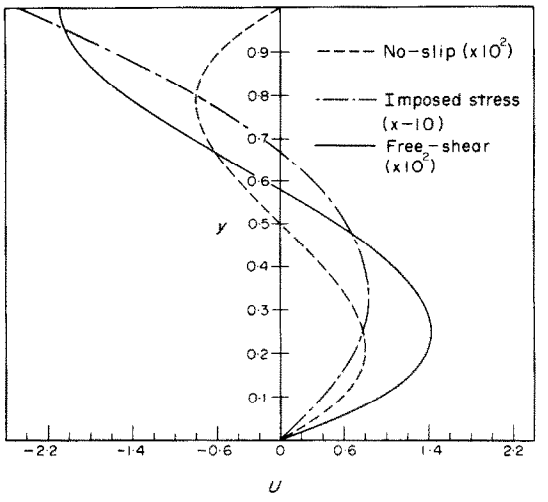

FIG. 3. Velocity profiles.

linearly additive shear induced velocity component $(3y^2/4 - y/2)$. Most significant are the variations in magnitude. Clearly, the free shear condition allows uniformly larger values of the horizontal velocity than does the no-slip condition. The normalized shear-induced velocity component is larger by an order of magnitude than even the corresponding free-shear component. Thus even for relatively small values of B, an imposed shear stress may have a significant influence on the circulation rate within the cavity. A comparison of equations (11) and (12) with equations (18) and (19) (with $B = 0$) reveals that the increased magnitude of the core velocity in the free surface problem, as compared to the no-slip problem, results in a smaller core temperature gradient (K_1), and an enhanced capacity for longitudinal transport of heat (Nu). In addition, the flow associated with a finite shear stress at the surface produces an additional correction to both K_1 and Nu whose sign depends on the magnitude and sign of B. It is especially significant that the convective contribution to Nu for the free surface case is approximately *five* times larger than the corresponding contribution for the no-slip problem, while the coefficients at $O(B)$ and $O(B^2)$ are both larger than the $O(1)$ coefficient by approximately an order of magnitude! Hence, even for small values of B, the convective transport of heat by Taylor diffusion may be *dominated* by the shear induced component of the flow.

The dependence of Nu on the shear parameter, B, is illustrated in Fig. 4, where the asymptotic solution for $(Nu - A)$ is plotted as a function of $Gr^2 Pr^2 A^3$ for various values of B. For comparison, the small A asymptote and the corresponding experimental data of Imberger [4] for the no-slip upper surface are also included. Three points are of special interest with regard to this figure. First, the asymptotic solution for $(Nu - A)$ shows an absolute minimum for fixed $Gr^2 Pr^2 A^3$, at $B = 0{\cdot}1458$. Second, comparison of the numerical solutions, experimental data and the asymptotic solution for the no-slip case seems to indicate that the asymptotic solutions will provide a reasonable approximation of the exact

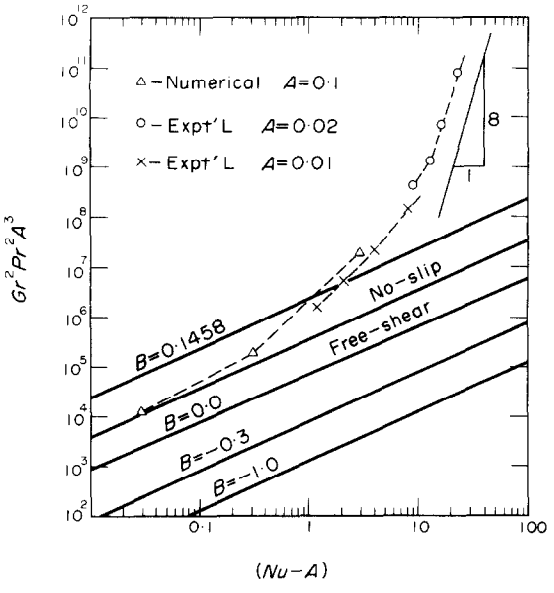

FIG. 4. $(Nu-A)$ vs $Gr^2Pr^2A^3$.

behavior for $A^3 < 10^5/Gr^2Pr^2$. Thus, the degree of shallowness required for validity of the present theory (i.e. the required value of A) decreases with decreasing Gr. Third, in the alternate limit, $Gr \to \infty$ with A held fixed (though small) the experimental data for various values of A approach one of a set of straight lines with slope of 1/8. This large Gr behavior is consistent with the boundary-layer analysis of Gill [11] which predicts (in terms of the ordinate of Fig. 4)

$$Nu = (cA^{-3/8})(Pr^2Gr^2A^3)^{1/8} \tag{20}$$

where c is a constant, independent of Gr, Pr and A. The numerical data of Quon [5] provide substantial evidence that the Nusselt number (and thus the constant, c) in this boundary-layer limit is the same for either a no-slip or free shear upper surface, in distinct contrast to the behavior in the present shallow cavity limit. Presumably, this difference reflects the fundamentally different physical processes governing the two limiting cases.

5. ASYMPTOTIC VELOCITY AND TEMPERATURE FIELDS WITH ZERO SURFACE SHEAR STRESS AND SPECIFIED HEAT FLUX

The discussion of Section 4 is intended to strongly emphasize the similarity in flow structure for the three kinematic surface conditions. In particular, the parallel nature of the core flow, the linearity of the temperature profiles and the similar form of the functions K_1 and Nu have been demonstrated. In contrast, the introduction of a heat flux at the top of the cavity can produce a fundamental change in the flow structure. For example, in the case of *strong* surface cooling, one would expect the slightly stable stratification that is produced in the insulated surface cases, to be destroyed. Ultimately, if the surface cooling is much greater than the total rate at which heat would be transferred through the end walls in the absence of surface cooling, a strongly unstable stratification must result, necessitating a major change in flow structure. For example, under appropriate circumstances, such cooling may lead to a modified "Benard" convection. In the alternate instance of strong surface *heating*, the slightly stable stratification of the insulated case would be intensified, thus tending to restrict free (vertical) movement of the fluid and cause a form of blocking as the stably stratified fluid encounters the end walls.

In considering these changes, it is convenient to associate the nonzero surface heat flux with a new length scale l', which is the distance required to transfer an amount of heat per unit time equal in magnitude to that exchanged at the end walls in the absence of surface heating. In general, it may be anticipated that, as an upper limit, the parallel flow structure discussed previously cannot be preserved over distances greater than l'. A comparison of l' with the physical length scale l of the cavity thus yields three limiting regimes, $l' \ll l$, $l' \sim l$ and $l' \gg l$ corresponding to the cases of large, moderate and small surface heat transfer. The case $l' \gg l$ is of only modest interest since it reduces, at first order, to the case of an insulated surface which we have previously considered. On the other hand, the case $l' \ll l$ leads to velocity and temperature distributions quite unlike those observed in the usual estuary flows. Hence, in the present discussion, we limit our considerations to the case $l' \sim l$ where the contributions of surface and end wall heat transfer are comparable.

(a) *Uniform surface heat flux*

In this section we consider the special case of constant, uniform surface heat transfer and zero surface shear stress. Thus, in (5), we put $\tau_0 = 0$ and $f(T) = q$ (constant), where q is the magnitude of the outwardly directed heat flux. In order that $l \sim l'$, as assumed, we require that the total heat flux per unit time through the upper surface of the cavity be of the same order of magnitude as the rate of heat exchange which would occur at the end walls in the absence of surface heating. Since the dimensionless heat flux through the end walls in the latter case is $O(A)$ [see equation (12)], it thus follows that the dimensionless heat flux at the upper surface must be restricted to be of $O(A^2)$, i.e.

$$\left.\frac{\partial\theta}{\partial y}\right|_{y=1} = -A^2Q \tag{21}$$

where

$$Q \equiv \frac{qh}{kA^2(T_h - T_c)}$$

is an arbitrary constant which is independent of A.

With the heat flux through the surface constrained, the scaling arguments that were outlined in Section 3 are still relevant and the core temperature and velocity fields are

$$\psi = \left\{Q\hat{x} + c_1 + A^2PrGrQ\left[\frac{Q(1-2\hat{x})}{1920} - \frac{1}{360}\right.\right.$$
$$\left.\left. + PrGr\left\{\left(\frac{Q^2}{24} - \frac{Q}{6} + \frac{1}{2}\right)1{\cdot}309 \times 10^{-5}\right.\right.\right.$$

$$-\left(\frac{Q^2\hat{x}^3}{3}+c_1Q\hat{x}^2+c_1^2\hat{x}\right)3{\cdot}927\times10^{-5}\Big\}\Big]\Big\}F'(y)$$
$$+A^2GrQ(Q\hat{x}+c_1)\left[\frac{y^9}{72\,576}-\frac{5y^8}{64\,512}+\frac{29y^7}{161\,280}\right.$$
$$-\frac{y^6}{4608}+\frac{y^5}{7680}-5{\cdot}977\times10^{-5}y^3+3{\cdot}049\times10^{-5}y^2$$
$$+Pr\left(\frac{y^9}{181\,440}-\frac{y^8}{32\,256}+\frac{y^7}{20\,160}-1{\cdot}740\times10^{-4}y^3\right.$$
$$\left.\left.+1{\cdot}498\times10^{-4}y^2\right)\right]+O(A^3) \quad (22a)$$

$$\theta=K_1\hat{x}+GrPrA^2K_1^2F(y)+K_2+\frac{Q\hat{x}^2}{2}-A^2Q\frac{y^2}{2}$$
$$+PrGrA^2(Q^2\hat{x}^2+2Qc_1\hat{x})F(y)-\frac{PrGrQ^2A^2\hat{x}^2}{1920}$$
$$-Pr^2Gr^2A^2Q\left(\frac{Q^2\hat{x}^4}{12}+\frac{Q\hat{x}^3c_1}{3}+\frac{c_1^2\hat{x}^2}{2}\right)$$
$$\times3{\cdot}927\times10^{-5}+O(A^4). \quad (22b)$$

As before, the coefficients of K_1 and K_2 were determined by matching with the relevant solutions in the end regions in a manner which proceeds as outlined in the Appendix. One important result is that the first order stream function in the end region is identical to the free-surface solution, ψ_0. However, in order to obtain K_1 and Nu correct to $O(A^3)$, it was necessary to obtain two *new* end region temperature solutions in addition to those outlined in the Appendix; one at $O(A^2)$ which can be expressed analytically, and one at $O(A^3)$ which must be determined numerically. The result for K_1‡ is

$$K_1=1-\frac{Q}{2}+PrGrA^2\left[\frac{Q^2}{1920}-\frac{2Q}{720}+PrGr\right.$$
$$\times\left(\frac{Q^3}{24}-\frac{Q^2}{6}+\frac{Q}{2}\right)3{\cdot}927\times10^{-5}\Big]+PrGrA^3$$
$$\times\left[Q\left(1-\frac{Q}{2}\right)2{\cdot}00\times10^{-3}-PrGr\right.$$
$$\left.\times\left(1-\frac{Q}{2}\right)^3 1{\cdot}916\times10^{-5}\right]+O(A^4). \quad (23)$$

As expected, equation (23) reduces to the insulated surface form [equation (18) with $B=0$] in the limit as $Q\to0$. However, for nonzero Q, K_1 is changed substantially even at $O(1)$. In addition, there is a correction to K_1 at $O(A^2)$, where previously there was no correction, as well as additional changes at $O(A^3)$. Unfortunately, the complex dependence of K_1 on Q prevents a more detailed comparison with previous results.

In all of the cases considered previously, the Nusselt number, as defined in Section 3, has provided a direct measure of the flux of heat between the end walls of the cavity. In contrast, however, the introduction of a flux of heat through the top of the cavity leads to a horizontal flux of heat that is a function of horizontal position. Nevertheless, either the hot or cold end Nusselt number does provide a measure of the overall dispersive capacity of the cavity for heat (the choice depends on whether the "source" is located at the hot or cold end of the cavity). The result in the cold end is

$$Nu_{\text{cold}}=\left(1-\frac{Q}{2}\right)A+A^3PrGr\left\{-Q^2 8{\cdot}68\times10^{-4}+Q\right.$$
$$\times\left(1-\frac{Q}{2}\right)1{\cdot}75\times10^{-2}+PrGr$$
$$\left.\times\left(\frac{Q^3}{4}-\frac{5Q^2}{4}+3Q-1\right)1{\cdot}31\times10^{-5}\right\}$$
$$+O(A^4) \quad (24)$$

and

$$Nu_{\text{hot}}=Nu_{\text{cold}}+QA.$$

Upon comparing Nu_{cold} and Nu_{hot} with the Nusselt number for an insulated surface [equation (18) with $B=0$], it may be observed that the heat enters through the hot end at a rate $(Q/2)A$ *slower* than it does for the insulated boundary case and leaves through the cold end at a rate $(Q/2)A$ *faster* than previously. Hence the heat added through the upper surface is "discharged" equally by the two ends of the cavity.

With the undetermined constants specified, it is possible to examine in detail the core streamfunction and temperature distributions. Notably the parallel flow structure that was so evident in the previous cases is no longer present. Even at first order in A, the streamlines are not parallel in the core

$$\psi^*=\left(Q\hat{x}+1-\frac{Q}{2}\right)F'(y)+O(A^2).$$

More surprising, however, for $|Q|>2$, the asymptotic theory predicts that the first order stream function vanishes at

$$\hat{x}_0=\frac{1}{2}-\frac{1}{Q}.$$

When $Q>2$, ψ^* is negative (clockwise circulation) for $\hat{x}<\hat{x}_0$ and positive (counterclockwise circulation) for $\hat{x}>\hat{x}_0$. On the other hand, when $Q<-2$, the opposite situation exists with counterclockwise circulation for $\hat{x}<\hat{x}_0$, and clockwise for $\hat{x}>\hat{x}_0$. This behavior of the first order velocity field, is intimately coupled with the first order temperature distribution

$$\theta^*=\left(1-\frac{Q}{2}\right)\hat{x}+Q\frac{\hat{x}^2}{2}+O(A^2).$$

A graphical comparison of the present temperature distribution and the previous insulated surface profile is shown in Fig. 5, where the first order temperature profiles are plotted for selected values of the surface heat flux. The positive values of Q represent surface cooling, hence the curves for $Q>0$ are shifted downward relative to the insulated surface curve ($Q=0$), while the curves for $Q<0$ are shifted upward. With sufficient cooling (or heating), temperatures smaller (larger) than the cold end (hot end) temperatures are

‡Note, $c_1=1-Q/2$.

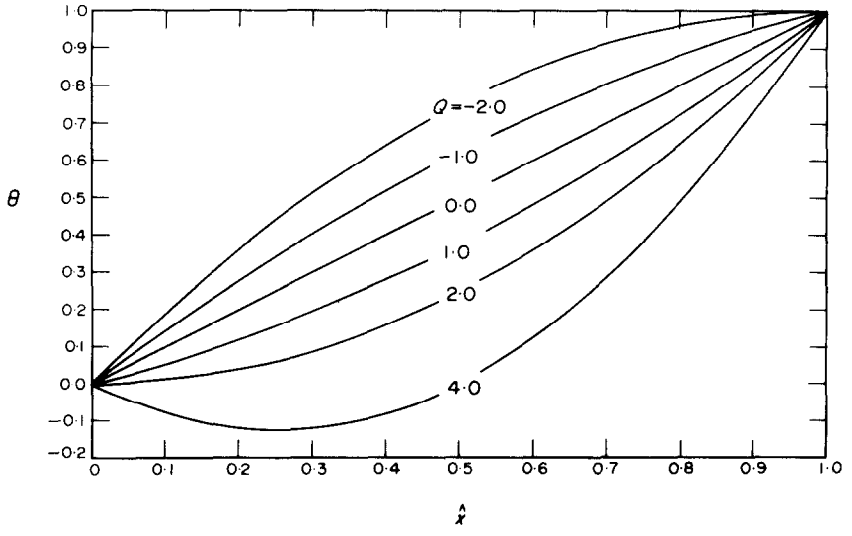

FIG. 5. First order temperature profile for uniform surface heat flux.

encountered within the cavity (cf. the curve for $Q = 4$). In particular, for $Q > 2$, θ^* has a negative gradient for $\hat{x} < \hat{x}_0$ and a positive gradient for $\hat{x} > \hat{x}_0$. The doubly circulating core flow encountered for $|Q| > 2$ is a result of this change in sign of the temperature gradient. Although this characteristic of the core flow is very interesting, it is clearly of limited relevance in the context of the estuary flow since such extreme surface cooling is unlikely to occur in the natural situation. Thus, it should be noted that if

$$Q \lesssim 1$$

then, as indicated in Fig. 5, the first order temperature and stream function profiles in the core are very similar to the insulated surface profiles, with the streamlines nearly parallel, and the horizontal temperature gradient practically constant.

(b) *Heat flux as a function of surface temperature*

The previous section dealt with a uniformly distributed surface heat flux. For an estuary this distribution of the heat flux is unrealistic since the net rate of heat exchange at any point on the surface is actually the sum of the rates at which heat is transferred by radiation, by evaporation, and by conduction between the water and the overlying air. Hence, the rate of heat transfer at each point on the surface must be specified as a function of the surface temperature as well as ambient variables such as wind speed, humidity and air temperature. Edinger, Duttweiler and Geyer [14] demonstrated that the net rate of heat transfer can be expressed most conveniently in terms of an effective thermal exchange coefficient K and an equilibrium temperature, T_e, both of which depend on observable meteorological variables and change continuously in response to varying meteorological conditions. The interested reader is referred to Edinger *et al.* [14] for details concerning the evaluation of K and T_e. The net heat-transfer rate becomes

$$q_{\text{net}} = -K(T_s - T_e)$$

where T_s is the surface temperature. For our present purposes we take T_e equal to the cold end temperature so that the surface heat flux is a maximum at $\hat{x} = 1$ and is a minimum (zero) at $\hat{x} = 0$, and assume that the surface shear stress is zero. As in the previous example, we consider only the case in which the total surface heat transfer is constrained to be of the same magnitude (with respect to A) as that which would occur at the end walls with $K \equiv 0$. Hence, we consider the boundary condition

$$\frac{\partial \theta}{\partial y} = -HA^2\theta \quad \text{on} \quad y = 1 \tag{25}$$

where

$$H \equiv \frac{Kh}{kA^2}$$

is an arbitrary constant which is independent of A.

To obtain an asymptotic solution for the core region, which is valid in the limit $A \to 0$ with Gr, Pr and H held fixed, we utilized the scaling arguments and formal expansion in A outlined previously. The core solution, after matching, is

$$\begin{aligned}\psi = {} & \left[\frac{(\sqrt{H})\cosh[(\sqrt{H})\hat{x}]}{\sinh(\sqrt{H})} + A^2 c_3'(\hat{x})\right] F'(y) + A^2 \\ & \times \left[\frac{\sinh[(\sqrt{H})\hat{x}]\cosh[(\sqrt{H})\hat{x}]}{\sinh^2(\sqrt{H})} H^{3/2} Gr\right. \\ & \times \left\{\frac{y^9}{72\,576} - \frac{5y^8}{64\,512} + \frac{29y^7}{161\,280} - \frac{y^6}{4608} + \frac{y^5}{7680}\right. \\ & - 5{\cdot}98 \times 10^{-5} y^3 + 3{\cdot}05 \times 10^{-5} y^2 + Pr\left(\frac{y^9}{181\,440}\right. \\ & - \frac{y^8}{32\,256} + \frac{y^7}{20\,160} - 1{\cdot}74 \times 10^{-5} y^3 \\ & \left.\left. + 1{\cdot}50 \times 10^{-4} y^2\right)\right\} - H^{3/2} \frac{\cosh[(\sqrt{H})\hat{x}]}{\sinh(\sqrt{H})} \\ & \left. \times \left\{\frac{y^6}{240} - \frac{y^5}{96} + \frac{y^4}{96} - \frac{y^3}{120} + \frac{y^2}{240}\right\}\right] + O(A^3)\end{aligned} \tag{26a}$$

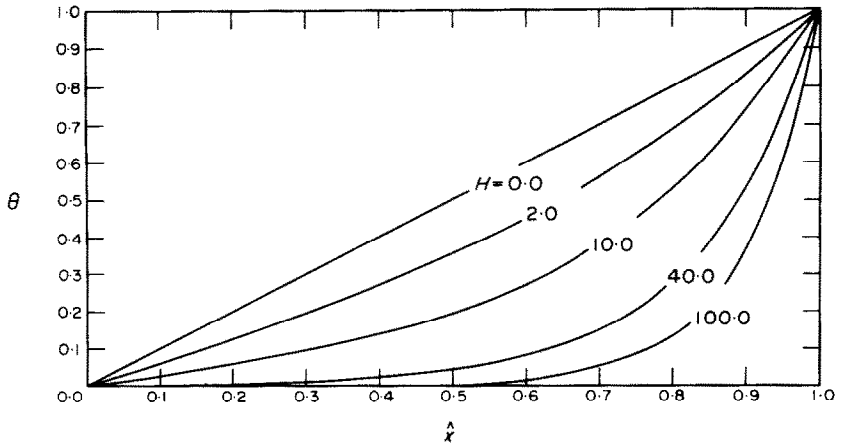

FIG. 6. First order temperature profile for surface heat flux a function of surface temperature.

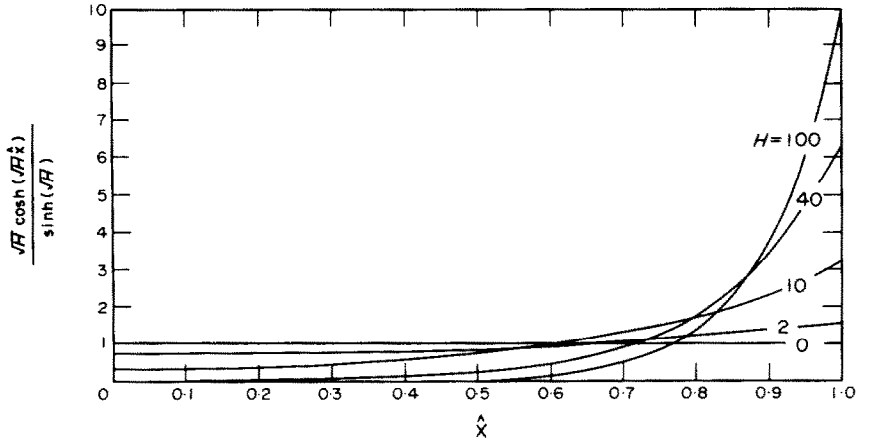

FIG. 7. Magnitude of first order stream function for surface heat flux a function of surface temperature.

$$\theta = \frac{\sinh[(\sqrt{H})\hat{x}]}{\sinh(\sqrt{H})} + A^2\left[-\frac{H\sinh[(\sqrt{H})\hat{x}]}{\sinh(\sqrt{H})}\frac{y^2}{2} + \frac{PrGrH\cosh^2[(\sqrt{H})\hat{x}]}{\sinh^2(\sqrt{H})}F(y) + c_3(\hat{x})\right] + O(A^3) \quad (26b)$$

where

$$c_3(\hat{x}) = \frac{PrGrH\cosh[2(\sqrt{H})\hat{x}]}{\sinh^2(\sqrt{H})5760} - \frac{3{\cdot}93\times10^{-5}Pr^2Gr^2}{\sinh^3(\sqrt{H})} \times\left\{\frac{H\sinh[3(\sqrt{H})\hat{x}]}{32} + \frac{H^{3/2}}{8}\hat{x}\cosh[(\sqrt{H})\hat{x}]\right\} - \frac{PrGrH}{640\sinh^2(\sqrt{H})} - \frac{H^{3/2}\hat{x}\cosh[(\sqrt{H})\hat{x}]}{6\sinh(\sqrt{H})} + \frac{\sinh[(\sqrt{H})\hat{x}]}{\sinh(\sqrt{H})}\left\{\frac{H}{6} + 3{\cdot}93\times10^{-5}\frac{Pr^2Gr^2}{\sinh^3(\sqrt{H})} \times\left[\frac{H\sinh(3\sqrt{H})}{32} + \frac{H^{3/2}\cosh(\sqrt{H})}{8}\right] - \frac{PrGrH}{576} + \frac{H^{3/2}\cosh(\sqrt{H})}{6\sinh(\sqrt{H})}\right\}.$$

As a result of the matching, it was also shown that the streamfunction for the cold end region is

$$\psi(x,y) = \frac{\sqrt{H}}{\sinh\sqrt{H}}\psi_0(x,y) + O(A^2), \quad (27)$$

while the hot end streamfunction is

$$\psi(A^{-1}-x,y) = (\sqrt{H})\coth(\sqrt{H})\psi_0(x,y) + O(A^2) \quad (28)$$

where ψ_0 is the same solution that was calculated for the zero shear case [Fig. 2(c)].

The behavior of the core solution in the limit as $H\to0$ is, of course, identical to the insulated surface case. An excellent indication of the influence of finite values of H is provided by the first order core solution. To facilitate discussion, we have plotted the first order temperature profile

$$\theta_0 = \frac{\sinh[(\sqrt{H})\hat{x}]}{\sinh(\sqrt{H})}$$

in Fig. 6 for selected values of H. In Fig. 7 we show

$$\frac{(\sqrt{H})\cosh[(\sqrt{H})\hat{x}]}{\sinh(\sqrt{H})}$$

(as an indication of the core streamfunction magnitude), for the same values of H. Because the surface heat flux

is proportional to the difference between surface temperature and T_c, a larger portion of the temperature drop occurs near the hot end of the cavity as H increases, thus causing increased temperature gradients in the hot end and decreased gradients in the cold end. These changes in the temperature profile are also reflected by the distribution of streamfunction in Fig. 7. The increased temperature gradient in the hot end increases the driving force for the core flow so that the streamfunction increases as H increases. The converse is true for the cold end. For the extreme case plotted, $H = 100$, ψ is essentially zero for $\hat{x} < 0{\cdot}5$. This tendency for ψ to approach zero at some distance far from the hot end wall hints of a limiting form of the solution as $H \to \infty$, in which A is no longer a relevant parameter. Since the flow field does not occupy the entire cavity, it must be unaware of the cold end wall and hence independent of the dimensionless cavity length, A^{-1}. In this sense, the flow behaves, for $H \to \infty$, as if the cavity were "semi-infinite". Figures 6 and 7 imply that the transition from "finite" to "semi-infinite" cavity occurs at $H \sim 40$.

Upon applying the limit $H \to \infty$ to the core solution (26), we obtain a limiting form which is independent of A as previously anticipated,

$$\lim_{H\to\infty} \psi = \sqrt{H}\left[\left\{e^{-\bar{\xi}} + \varepsilon^2\left(\frac{2PrGr\,e^{-2\xi}}{5760} - 3{\cdot}68\times10^{-6}Pr^2Gr^2e^{-3\xi} + \xi\frac{e^{-\xi}}{6} + e^{-\xi}\left(1{\cdot}23\times10^{-6}Pr^2Gr^2 - \frac{PrGr}{576}\right)\right)\right\}F'(y) + \varepsilon^2\left\{e^{-2\xi}Gr\left(\frac{y^9}{72\,576} - \frac{5y^8}{64\,512} + \frac{29y^7}{161\,280} - \frac{y^6}{4608} + \frac{y^5}{7680} - 5{\cdot}98\times10^{-4}y^3 + 3{\cdot}05\times10^{-5}y^2 + Pr\left(\frac{y^9}{181\,440} - \frac{y^8}{32\,256} + \frac{y^7}{20\,160} - 1{\cdot}74\times10^{-5}y^3 + 1{\cdot}50\times10^{-4}y^2\right)\right)\right\} + O(\varepsilon)^3\right] \quad (29a)$$

$$\lim_{H\to\infty} \theta = e^{-\xi} + \varepsilon^2\left[-e^{-\xi}\frac{y^2}{2} + PrGr\,e^{-2\xi}F(y) + \frac{PrGr\,e^{-2\xi}}{5760} - 1{\cdot}23\times10^{-6}Pr^2Gr^2e^{-3\xi} + \frac{\xi e^{-\xi}}{6} + e^{-\xi}\left\{\frac{1}{6} + 1{\cdot}23\times10^{-6}Pr^2Gr^2 - \frac{PrGr}{576}\right\}\right] + O(\varepsilon^3) \quad (29b)$$

in which

$$\bar{\xi} = \varepsilon\xi \quad \text{and} \quad \varepsilon \equiv \sqrt{\left(\frac{Kh}{k}\right)}.$$

For convenience, we have used the independent variable ξ which measures the horizontal distance into the cavity from the hot end, scaled with respect to h.

In view of the expressions (27)–(29), it is apparent that the appropriate velocity and length scales in the limit $H \to \infty$ are

$$u = O\left[\left(\sqrt{\frac{Kh}{k}}\right)\frac{\beta g(T_h - T_c)h^3}{\nu}\right]$$

and (30)

$$l' = O\left(\frac{h}{\varepsilon}\right) = O\left[\sqrt{\left(\frac{kh}{K}\right)}\right].$$

The latter is the length scale characterizing the rate of heat transfer through the cavity surface. This spontaneous appearance of a new length scale provides an excellent opportunity to enlarge on the previous discussion relating the horizontal length scale of the core flow to the rate of surface cooling. To this end, Fig. 8 shows the fully matched first order streamfunction profiles for the semi-infinite cavity ($H \to \infty$) at two values of ε. It is clear from these figures that as the heat transfer rate (ε^2) increases, the horizontal extent of the core flow is decreased proportionately.

An examination of the semi-infinite cavity solution (equations 29) indicates that to ensure convergence, we must have $\varepsilon \ll 1$. This in turn suggests that a necessary condition for the validity of the analysis leading to the general solutions (26) is

$$A \ll 1$$

and

$$HA^2 = \frac{Kh}{k} \ll 1.$$

To determine if the second inequality will be satisfied under realistic conditions, it is useful to estimate the magnitude of Kh/k. Field measurements indicate that, for an ambient wind speed of from 1 to 5 m/s, K varies between about $2{\cdot}5\times10^{-4}$ and $5{\cdot}0\times10^{-3}$ cal(c°cm²s)$^{-1}$. Furthermore, since estuary flows are invariably turbulent, we estimate the effective thermal diffusivity to be of the order u^*h† (cf. Fischer [12]), where u^* is the "slip velocity" and is about 1 cm/s for horizontal fluid velocities of about 10 cm/s. (The precise magnitude of the horizontal velocity will depend on Gr, Pr, A and H.) Hence,

$$\frac{Kh}{k} \sim 10^{-4}$$

for typical estuary flows.

The heat-transfer characteristics for the present surface boundary condition are quite different from the insulated surface case. Once again, because heat is removed through the surface of the cavity, the horizontal heat flux is a function of horizontal position. The

† Here we have assumed that the turbulent Prandtl number is ~1.

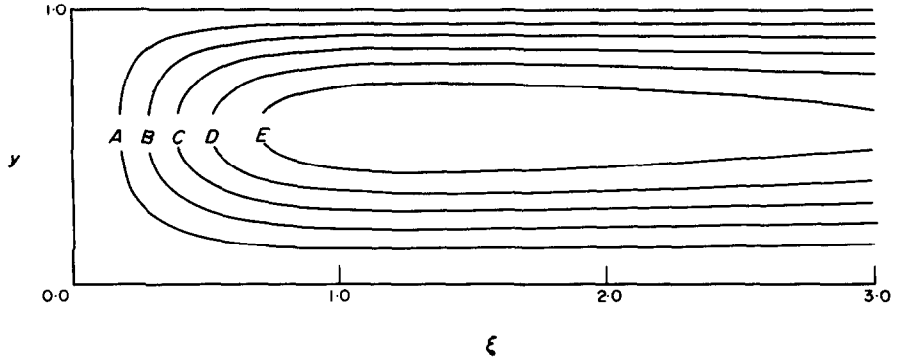

(a) $\varepsilon = 0{\cdot}1$; $A = 7{\cdot}7 \times 10^{-4}$, $B = 1{\cdot}5 \times 10^{-3}$, $C = 2{\cdot}3 \times 10^{-3}$, $D = 3{\cdot}1 \times 10^{-3}$, $E = 3{\cdot}8 \times 10^{-3}$.

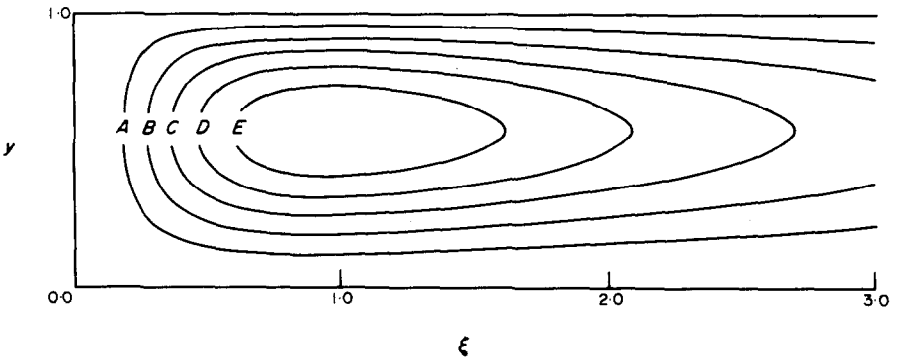

(b) $\varepsilon = 0{\cdot}5$; $A = 4{\cdot}4 \times 10^{-4}$, $B = 9{\cdot}3 \times 10^{-4}$, $C = 1{\cdot}4 \times 10^{-3}$, $D = 1{\cdot}9 \times 10^{-3}$, $E = 2{\cdot}4 \times 10^{-3}$.

FIG. 8. Streamlines for semi-infinite cavity.

Nusselt number is therefore a maximum at the hot end

$$Nu_{\text{hot}} = A(\sqrt{H})\coth(\sqrt{H}) + A^3\Bigg[PrGrH^{3/2}\Bigg(\frac{\coth(\sqrt{H})}{960} + \frac{\sinh(2\sqrt{H})}{2880\sinh(\sqrt{H})}\Bigg) - \frac{H^{3/2}}{6}\coth(\sqrt{H}) - 3{\cdot}927\times10^{-5}\frac{Pr^2Gr^2}{\sinh^3(\sqrt{H})}\Bigg\{\frac{H^2}{8}\sinh(\sqrt{H}) - \sqrt{H}\coth(\sqrt{H})\Bigg\{\frac{H}{32}\sinh(3\sqrt{H}) + \frac{H^{3/2}}{8}\cosh(\sqrt{H})\Bigg\} + \frac{3H^{3/2}}{32}\cosh(3\sqrt{H}) + \frac{H^{3/2}}{8}\cosh(\sqrt{H})\Bigg\} - \frac{H}{6}(1-\coth^2(\sqrt{H})) + PrGrH^{3/2}\{1{\cdot}309\times10^{-5}PrGr\coth^3(\sqrt{H}) - 1{\cdot}74\times10^{-3}\coth(\sqrt{H})\}\Bigg] + O(A^4) \quad (31)$$

and is a minimum at the cold end

$$Nu_{\text{cold}} = \frac{A\sqrt{H}}{\sinh(\sqrt{H})} + A^3\Bigg[-\frac{H^{3/2}}{\sinh(\sqrt{H})}\Bigg(\frac{1}{6} + 8{\cdot}59\times10^{-6}\frac{Pr^2Gr^2}{\sinh^2(\sqrt{H})} + \frac{PrGr}{576} - \frac{Pr^2Gr^2(1{\cdot}309\times10^{-5})}{\sinh^2(\sqrt{H})} - 1{\cdot}227\times10^{-6}\times\frac{Pr^2Gr^2}{\sinh^3(\sqrt{H})}\sinh(3\sqrt{H})\Bigg) + 4{\cdot}91\times10^{-6}\times\frac{Pr^2Gr^2H^2}{\sinh^4(\sqrt{H})}\cosh(\sqrt{H}) + H^2\frac{\coth(\sqrt{H})}{6\sinh(\sqrt{H})}\Bigg] + O(A^4). \quad (32)$$

In the limit as $H \to 0$, these expressions for Nu reduce to that found for the insulated free-shear surface. Unfortunately, the complexity of expressions (31) and (32) precludes a detailed comparison with Nusselt numbers for the previous cases.

REFERENCES

1. W. B. Logan and D. E. Cebulski, Carbonate sedimentation and environments, Shark Bay, Western Australia, The American Ass. of Pet. Geol., Memoir No. 13 (1970).
2. H. B. Fischer, Mass transport mechanisms in partially stratified estuaries, *J. Fluid Mech.* **53**, 671 (1972).
3. D. R. F. Harleman and K. D. Stolzenbach, Fluid mechanics of heat disposal from power generation, *Ann. Rev. Fluid Mech.* **4**, 7 (1972).
4. J. Imberger, Natural convection in a shallow cavity with differentially heated end walls. Part 3. Experimental results, *J. Fluid Mech.* **65**, 247 (1974).
5. C. Quon, High Rayleigh number convection in an enclosure—a numerical study, *Physics Fluids* **15**, 12 (1972).
6. J. O. Wilkes and S. W. Churchill, The finite difference computation of natural convection in a rectangular enclosure, *A.I.Ch.E. Jl* **12**, 161 (1966).

7. M. E. Newell and F. W. Schmidt, Heat transfer by laminar natural convection within rectangular enclosures, *J. Heat Transfer* **92**, 159 (1970).
8. G. DeVahl Davis, Laminar natural convection in an enclosed rectangular cavity, *Int. J. Heat Mass Transfer* **11**, 1675 (1968).
9. D. E. Cormack, L. G. Leal and J. Imberger, Natural convection in a shallow cavity with differentially heated end walls. Part 1. Asymptotic theory, *J. Fluid Mech.* **65**, 209 (1974).
10. D. E. Cormack, L. G. Leal and J. H. Seinfeld, Natural convection in a shallow cavity with differentially heated end walls. Part 2. Numerical solutions, *J. Fluid Mech.* **65**, 231 (1974).
11. A. E. Gill, The boundary-layer regime for convection in a rectangular cavity, *J. Fluid Mech.* **26**, 515 (1966).
12. H. B. Fischer, Longitudinal dispersion and turbulent mixing in open channel flows, *Ann. Rev. Fluid Mech.* **5**, 59 (1973).
13. J. L. Lumley and H. A. Panofsky, *The Structure of Atmospheric Turbulence*. Interscience, New York (1964).
14. J. E. Edinger, D. W. Duttweiler and J. C. Geyer, The response of water temperature to meteorological conditions, *Water Res.* **4**, 1137 (1968).

APPENDIX A

To demonstrate the matching procedure used in the paper, we consider the simplest case, that of an insulating, free surface ($\tau_0 = 0$) at the top of the cavity. Subject to the assumption that the surface is flat, boundary conditions (5) become

$$\psi = \frac{\partial^2\psi}{\partial y^2} = \frac{\partial\theta}{\partial y} = 0 \quad \text{on} \quad y = 1. \tag{A.1}$$

The problem is otherwise the same as that outlined in Section 3, and the horizontal scaling arguments remain valid. Thus, the core solution consistent with the conditions (A.1) may easily be shown to be

$$\psi = K_1\left(\frac{y^4}{24} - \frac{5y^3}{48} + \frac{y^2}{16}\right) \tag{A.2}$$

$$\theta = K_1\hat{x} + K_1^2 GrPrA^2\left(\frac{y^5}{120} - \frac{5y^4}{192} + \frac{y^3}{48}\right) + K_2. \tag{A.3}$$

Both K_1 and K_2 are polynomials in A, with coefficients which must be determined by matching (A.2) and (A.3) with solutions which are valid in the ends of the cavity. For the no-slip surface, the centro-symmetry property of the equations and boundary conditions allowed K_2 to be eliminated in favor of K_1, so that the matching had to be carried out explicitly only in the cold end of the cavity. In the present example, and, indeed, in all of the problems considered in the present work, this simplification is not possible so that it is necessary, in principle, to carry out the detailed matching explicitly in both ends of the cavity. As we shall see, however, certain symmetry relationships are still useful in simplifying the problem.

In the cold end, the original equations (1), (2) and (3) must be solved, subject to the boundary conditions (4) and (A.1) for $y = 0$, 1 and $x = 0$, so that they match with the core solution according to

$$\lim_{x\to\infty}\psi = (c_1 + Ac_2 + \ldots)F'(y) \tag{A.4}$$

$$\lim_{x\to\infty}\theta = (c_1 + Ac_2 + \ldots)\hat{x} + (c_1 + Ac_2 + \ldots)^2 GrPrA^2 F(y) + (c_1' + Ac_2' + \ldots). \tag{A.5}$$

Here

$$F(y) = \frac{y^5}{120} - \frac{5y^4}{192} + \frac{y^3}{48}$$

and the prime in $F'(y)$ denotes differentiation with respect to y.

In the hot end of the cavity, it is convenient to express the equations and matching conditions in terms of the transformed variables

$$\xi = (A^{-1} - x)$$
$$\eta = (1 - y)$$
$$\Theta = 1 - \theta$$

so that the form of the equations remains unchanged

$$GrA^2\frac{\partial(\Omega,\Psi)}{\partial(\xi,\eta)} = A\nabla^2\Omega + \frac{\partial\Theta}{\partial\xi} \tag{A.6}$$

$$\nabla^2\Psi = -\Omega \tag{A.7}$$

$$PrGrA\frac{\partial(\Theta,\Psi)}{\partial(\xi,\eta)} = \nabla^2\Theta \tag{A.8}$$

but the boundary conditions become

$$\left.\begin{aligned}
&\Psi = \frac{\partial\Psi}{\partial\xi} = \Theta = 0 \quad \text{on} \quad \zeta = 0\\
&\Psi = \frac{\partial\Psi}{\partial\eta} = \frac{\partial\Theta}{\partial\eta} = 0 \quad \text{on} \quad \eta = 1\\
&\Psi = \frac{\partial^2\Psi}{\partial\eta^2} = \frac{\partial\Theta}{\partial\eta} = 0 \quad \text{on} \quad \eta = 0.
\end{aligned}\right\} \tag{A.9}$$

Here, Ψ and Ω denote the stream function and vorticity in the hot end. The transformed matching conditions are

$$\lim_{\xi\to\infty}\Psi = (c_1 + Ac_2 + \ldots)F'(1-\eta)$$

$$\lim_{\xi\to\infty}(1-\Theta) = (c_1 + Ac_2 + \ldots)(1 - \xi A) + (c_1 + Ac_2 + \ldots)^2 GrPrA^2 F(1-\eta) + (c_1' + Ac_2' + \ldots).$$

A solution in each of the hot and cold ends can be obtained as a regular expansion in A, i.e.

$$\psi = \psi_0 + A\psi_1 + \ldots; \quad \theta = \theta_0 + A\theta_1 + \ldots \quad \text{(cold)}$$
$$\Psi = \Psi_0 + A\Psi_1 + \ldots; \quad \Theta = \Theta_0 + A\Theta_1 + \ldots \quad \text{(hot)}$$

We have listed the appropriate equations and matching conditions at each order in A in Table 1.

To initiate the solution of these equations, we note that the temperature functions θ_0 and Θ_0 are both identically zero, so that to satisfy the matching constraints (C1) and (H1) it follows that

$$c_1' = 0$$
$$c_1 = 1.$$

Because θ_0 is zero, equation (C3) reduces to $\nabla^2\theta_1 = 0$ and can be solved independently from (C2) to yield

$$\theta_1 = x$$

with the corresponding result from the matching condition (C5)

$$c_2' = 0.$$

Similarly, in the hot end,

$$\Theta_1 = \xi$$

and the condition (H5) yields

$$c_2 = 0.$$

In light of these results, equations (C2) and (H2) may now be solved to yield the $O(1)$ contributions to the flow field in the hot and cold end. Substituting the solutions for θ_1 and Θ_1 into these equations, we obtain for the cold end

$$\nabla^4\psi_0 = 1 \tag{A.10}$$

with matching condition

$$\lim_{x\to\infty}\psi_0 \to F'(y),$$

Table 1. End region equations and matching conditions for $\tau_0 = 0$

	Cold end		Hot end	
$O(1)$	$\dfrac{\partial\theta_0}{\partial x} = 0$		$\dfrac{\partial\Theta_0}{\partial\xi} = 0$	
	$\lim_{x\to\infty}\theta_0 = C_1'$	(C1)	$\lim_{\xi\to\infty}\Theta_0 = 1-C_1-C_1'$	(H1)
	$\nabla^2\theta_0 = 0$		$\nabla^2\Theta_0 = 0$	
$O(A)$	$\nabla^4\psi_0 = \dfrac{\partial\theta_1}{\partial x}$	(C2)	$\nabla^4\psi_0 = \dfrac{\partial\Theta_1}{\partial\xi}$	(H2)
	$\nabla^2\theta_1 = PrGr\dfrac{\partial(\theta_0,\psi_0)}{\partial(x,y)}$	(C3)	$\nabla^2\Theta_1 = PrGr\dfrac{\partial(\Theta_0,\Psi_0)}{\partial(\xi,\eta)}$	(H3)
	$\lim_{x\to\infty}\psi_0 = C_1F'(y)$	(C4)	$\lim_{\xi\to\infty}\Psi_0 = C_1F'(1-\eta)$	(H4)
	$\lim_{x\to\infty}\theta_1 = C_1x+C_2'$	(C5)	$\lim_{\xi\to\infty}\Theta_1 = C_1\xi-C_2-C_2'$	(H5)
$O(A^2)$	$\nabla^4\psi_1 = \dfrac{\partial\theta_2}{\partial x} - Gr\dfrac{\partial(\omega_0,\psi_0)}{\partial(x,y)}$	(C6)	$\nabla^4\Psi_1 = \dfrac{\partial\Theta_2}{\partial\xi} - Gr\dfrac{\partial(\Omega_0,\Psi_0)}{\partial(\xi,\eta)}$	(H6)
	$\nabla^2\theta_2 = PrGr\left[\dfrac{\partial(\theta_1,\psi_0)}{\partial(x,y)}+\dfrac{\partial(\theta_0,\psi_1)}{\partial(x,y)}\right]$	(C7)	$\nabla^2\Theta_2 = PrGr\left[\dfrac{\partial(\Theta_1,\Psi_0)}{\partial(\xi,\eta)}+\dfrac{\partial(\Theta_0,\Psi_1)}{\partial(\xi,\eta)}\right]$	(H7)
	$\lim_{x\to\infty}\psi_1 = C_2F'(y)$	(C8)	$\lim_{\xi\to\infty}\Psi_1 = C_2F'(1-\eta)$	(H8)
	$\lim_{x\to\infty}\theta_2 = C_2x+C_1^2GrPrF(y)+C_3'$	(C9)	$\lim_{\xi\to\infty}\Theta_2 = C_2\xi-C_1^2GrPrF(1-\eta)-C_3'-C_3$	(H9)
$O(A^3)$	$\nabla^4\psi_2 = \dfrac{\partial\theta_3}{\partial x} - Gr\left[\dfrac{\partial(\omega_0,\psi_1)}{\partial(x,y)}+\dfrac{\partial(\omega_1,\psi_0)}{\partial(x,y)}\right]$	(C10)	$\nabla^4\Psi_2 = \dfrac{\partial\Theta_3}{\partial\xi} - Gr\left[\dfrac{\partial(\Omega_0,\Psi_1)}{\partial(\xi,\eta)}+\dfrac{\partial(\Omega_1,\Psi_0)}{\partial(\xi,\eta)}\right]$	(H10)
	$\nabla^2\theta_3 = PrGr\left[\dfrac{\partial(\theta_1,\psi_1)}{\partial(x,y)}+\dfrac{\partial(\theta_2,\psi_0)}{\partial(x,y)}+\dfrac{\partial(\theta_0,\psi_2)}{\partial(x,y)}\right]$	(C11)	$\nabla^2\Theta_3 = PrGr\left[\dfrac{\partial(\Theta_1,\Psi_1)}{\partial(\xi,\eta)}+\dfrac{\partial(\Theta_2,\Psi_0)}{\partial(\xi,\eta)}+\dfrac{\partial(\Theta_0,\Psi_2)}{\partial(\xi,\eta)}\right]$	(H11)
	$\lim_{x\to\infty}\psi_2 = C_3F'(y)$	(C12)	$\lim_{\xi\to\infty}\Psi_2 = C_3F'(1-\eta)$	(H12)
	$\lim_{x\to\infty}\theta_3 = C_3x+2C_1C_2GrPrF(y)+C_4'$	(C13)	$\lim_{\xi\to\infty}\Theta_3 = C_3\xi-C_4-2C_1C_2GrPrF(1-\eta)-C_4'$	(H13)

and for the hot end

$$\nabla^4\Psi_0 = 1$$

with

$$\lim_{\xi\to\infty}\Psi_0 \to F'(1-\eta).$$

From these equations, it is clear that the hot end stream function, Ψ_0, can be expressed in terms of the cold end distribution by

$$\psi_0(\alpha,\gamma) = \Psi_0(\alpha,1-\gamma).$$

It is therefore necessary to obtain only one of the hot or cold end solutions at this level of approximation. We consider the function ψ_0 in the cold end.

We have shown in [9] that it is possible to obtain an analytical solution for ψ_0. However, the resulting solution is extremely cumbersome and becomes completely unwieldy for evaluating higher order solutions. On the other hand, numerical solution of equation (A.10) with appropriate boundary conditions is relatively straightforward and for the present purposes is sufficient. In order to obtain this solution, the equation (A.10) was approximated by a central difference representation on a geometrically expanding grid of twenty-one points in the x-direction and a uniform grid of twenty-one points in the y-direction and solved using an explicit Gauss–Seidel iterative scheme. Details of the calculation may be obtained from [9]. The resulting streamlines of ψ_0 are presented in Fig. 2(c).

We turn now to consider the solution at $O(A^2)$ for θ. Taking the preceding results into account, the governing equation (C5) in the cold end becomes

$$\nabla^2\theta_2 = PrGr\frac{\partial\psi_0}{\partial y} \tag{A.11}$$

with the matching condition

$$\lim_{x\to\infty}\theta_2 = GrPrF(y)+c_3'.$$

The matching at this order in A can be accomplished most effectively by considering the integral of equation (A.11) over the depth of the cavity. Carrying out this integration, we obtain the ordinary differential equation for

$$H(x) \equiv \int_0^1 \theta_2\,dy$$

$$\frac{d^2H}{dx^2} = 0 \tag{A.12}$$

with the integrated boundary conditions

$$H = 0 \quad \text{on} \quad x = 0 \tag{A.13a}$$

$$\lim_{x\to\infty}H = GrPr\int_0^1 F(y)\,dy + c_3'. \tag{A.13b}$$

The only solution of equation (A.12) consistent with the conditions (A.13) is the trivial solution

$$H = 0$$

for all x. Hence, it follows that

$$c_3' = -GrPr\int_0^1 F(y)\,dy = -\frac{GrPr}{720}.$$

A similar integral analysis of equation (H5) indicates that

$$c_3 = 0.$$

In order to carry the asymptotic solution to higher orders in A, it is necessary to determine the detailed distribution of θ_2 in the end region. This was done using the same numerical procedure and grid spacing as described previously for ψ_0. It may also appear that an independent numerical solution must be obtained for Θ_2; however, this is not the case. Rather, by considering the relationship between ψ_0 and Ψ_0 and the relationship between the boundary conditions on θ_2 and Θ_2, it is possible to show that

$$\theta_2(\alpha,\gamma) = -\Theta_2(\alpha,1-\gamma).$$

Finally, it would now be possible to obtain a numerical solution for ψ_1. However, our main interest in continuing the expansion to higher order in A is to obtain the first nontrivial corrections to K_1 and Nu. For this purpose, it is sufficient to note that ψ_1 must satisfy the condition

$$\lim_{x\to\infty}\psi_1 = 0.$$

The first nonzero correction to K_1 comes from the coefficient c_4 (note $c_2 = c_3 = 0$). To obtain c_4, we must consider the problem (C7) and (C9) for θ_3. This equation, plus matching condition, is simplified by our preceding results to

$$\nabla^2\theta_3 = PrGr\left[\frac{\partial\psi_1}{\partial y} + \frac{\partial(\theta_2,\psi_0)}{\partial(x,y)}\right] \tag{A.14}$$

with

$$\lim_{x\to\infty}\theta_3 = c_4'.$$

Utilizing the linearity of this problem, we can conveniently consider θ_3 and c_4' as consisting of two parts

$$\theta_3 = \bar{\theta}_3 + \bar{\bar{\theta}}_3$$

and

$$c_4' = \bar{c}_4' + \bar{\bar{c}}_4'$$

where

$$\nabla^2\bar{\theta}_3 = PrGr\frac{\partial\psi_1}{\partial y} \tag{A.15}$$

with

$$\lim_{x\to\infty}\bar{\theta}_3 = \bar{c}_4'$$

and

$$\nabla^2\bar{\bar{\theta}}_3 = PrGr\frac{\partial(\theta_2,\psi_0)}{\partial(x,y)} \tag{A.16}$$

with

$$\lim_{x\to\infty}\bar{\bar{\theta}}_3 = \bar{\bar{c}}_4'.$$

A consideration of the integral of equation (A.15) across the depth of the cavity yields the result

$$\int_0^1 \bar{\theta}_3\,dy \equiv 0$$

for all x, so that

$$\bar{c}_4' = 0.$$

On the other hand, such an integral analysis of equation (A.16) yields no information concerning $\bar{\bar{c}}_4'$. Instead, $\bar{\bar{c}}_4'$ must be determined by numerically solving equation (A.16) subject to the boundary condition (see [9])

$$\lim_{x\to\infty}\frac{\partial\bar{\bar{\theta}}_3}{\partial x} = 0.$$

This procedure yields both the unique solution for $\bar{\bar{\theta}}_3$, and the numerical value

$$\bar{\bar{c}}_4' = 9{\cdot}58\times10^{-6}Gr^2Pr^2.$$

In the same manner that the relationship between θ_2 and Θ_2 was deduced previously, it is also possible to show that

$$\bar{\bar{\theta}}_3(\alpha,\gamma) = \bar{\bar{\Theta}}_3(\alpha,1-\gamma).$$

In particular, therefore, the matching condition for Θ_3 requires

$$c_4 = -2\bar{\bar{c}}_4'.$$

This completes the solution to the desired level of approximation.